Robust estimation of the motile cilia beating frequency

Olivier Meste, Frédéric Brau, Alice Guyon

Noname manuscript No.
(will be inserted by the editor)

Robust Estimation of the Motile Cilia Beating Frequency

O. MESTE · F. BRAU · A. GUYON

Abstract The estimation of the cilia beating frequency (CBF) is of great interest in understanding how the CBF modulates liquid fluxes and how it is controlled by the ciliated cell intra- and/or extra-cellular medium composition in physiological processes. Motion artifacts and camera defaults may hinder the computation of the frequency variations during long lasting experiments. We have developed a new analysis approach consisting of a preliminary corrective step (removal of a grid pattern on the image sequence and shift compensation), followed by a harmonic model of the observed cilia using a Maximum Likelihood Estimator framework.

O. MESTE
Lab I3S, CNRS University of Nice-Sophia Antipolis
E-mail: meste@unice.fr

F. BRAU
IPMC, CNRS University of Nice-Sophia Antipolis
E-mail: brau@ipmc.cnrs.fr

A. GUYON
IPMC, CNRS University of Nice-Sophia Antipolis
E-mail: aguyon@ipmc.cnrs.fr

It is shown that a more accurate estimation of the frequency can be obtained by averaging the squared Fourier transform of individual pixels followed by a particular summation over the different frequencies, namely the Compressed Spectrum. Robustness of the proposed method over traditional approaches is shown by several examples and simulations. The method is then applied to images of samples containing ciliated ependymal cells located in the third cerebral ventricle of mouse brains, showing that even small variations in CBF in response to changes in the amount of oxygenation, pH or glucose were clearly visible in the computed frequencies. As a conclusion, this method reveals a fine metabolic tuning of the cilia beating in ependimocytes lining the third cerebral ventricle. Such regulations are likely to participate in homeostatic mechanisms regulating CSF movements and brain energy supply.

Keywords: Signal Processing, Cilia, Frequency Estimation

1 Introduction

Motile cilia play a crucial role in fluid circulation in many biological systems such as the oviduct, the airway and the cerebral ventricles. Defects in cilia beating lead to pathologies called ciliopathies [1]. For instance, in the third ventricle of the brain cavities, motile cilia play a major role in circulating cerebro-spinal fluid (CSF), where abnormal ciliary beating has recently been linked to hydrocephalus and other developmental cerebral abnormalities. In addition, they are thought to be a part of the central glucose sensing system [2]. In both cases, circulation and clearing are performed by movements of the cerebro-spinal fluid via the coordination of the beating cilia. Beating properties are usually addressed by the inverse of the time

period, namely the Ciliary Beating Frequency (CBF). This frequency is strongly affected by the molecular components of the cells and the submerging fluid, thus contributing to local homeostatic processes. By this way, CBF changes may allow the indirect assessment of metabolic variation. It is clear that greater accuracy in the estimation of these changes will allow precise measurements to be made of the more subtle variations of CBF in response to changes in the medium.

Unfortunately, different factors hinder the estimation of CBF changes. First, cilia are densely packed on all naturally occurring ciliated surfaces (Fig. 1 and Fig. 2). Since this density is observed in the three dimensional case, classical imaging systems will fail to track a single cilium for CBF analysis purpose. Frame-by-frame line tracing [14] computed by heavy manual intervention can allow cilia tracking for motility analysis. Second, the recorded image will be a combination of overlapping cilia, likely beating at slightly different frequencies. Third, CBF measurements need to be automated because of the length of experiments due to long time constants of the CBF changes following the tested molecular component variations. Forth, because of both the fluid flux generated by the cilia and the solution flow perfusing the slices during recordings, the samples recorded with the image acquisition system shift geometrically from frame to frame. Finally, permanent patterns such as the grid line image artifacts due to the CMOS camera acquisition system might be recorded during the experiment and hinder correct image registration.

Those limitations are mostly due to the acquisition equipment and procedure. Many studies focused on improving the acquisition devices. However, advanced frequency estimation techniques are available and they could help to overcome those limitations by using adequate pre-processing. Indeed, this problem cannot

be efficiently approached using image processing tools such as pattern detection and tracking because of the overlapping cilia. Attempts based on optical flow [3] and correlation methods [4] failed when measuring the CBF in cilia from the brain slices at our disposal (where cilia are intermingled and beat with a high frequency), giving instable and noisy measures. A robust CBF estimator that combines advantageously the temporal and spatial properties of the cilia is needed. In this respect, standard signal processing tools as Fourier analysis [5] may be helpful. Recent studies have proposed methods based on visual inspection [6], classical Fourier analysis [6] [9] and pixel average [6] [7] [8]. However, for long experiments, frequencies computed from visual measurement have to be used carefully because of potential bias. Moreover, those methods do not fully exploit the underlying physiological model in terms of cilia properties when considering traditional Fourier analysis. In this respect, harmonicity of the frequency content of the cilia movements has been pointed out in [10] but not fully exploited in order to increase the accuracy of the CBF estimation.

This study proposes a new method for CBF estimation. The method first removes grid artefacts, as described in section 2.2 and then compensates for the geometrical sample shift. In section 2.3, a full derivation of our approach is provided, including theoretical development and comparison to Fourier based analysis and validated with simulated data and illustrative examples. We show the optimality of averaging the squared modulus of the Fourier Transform provided that the pixels share the same temporal behavior, even when phase-shifted. In addition, the modeling of the periodic temporal pattern observed on each pixel is addressed through harmonic decomposition leading to the use of the Compressed Spectrum. In addition to already available results, in section 2.4 the method is

used to demonstrate the changes in cilia beating frequency in response to various metabolic changes in ependymal cells, lining the third ventricle of the brain cavity. Finally, this work will be ended by a discussion.

2 Methods

2.1 Image acquisition

2.1.1 Brain slices

All the protocols were carried out in accordance with the French standard ethical guidelines for laboratory animals (Agreement N 75-178, 05/16/2000) and were approved by the IPMC care committee. Attention was paid to use only the number of animals required to generate reproducible results. 12-80 day old male wild type C57BL6 mice were bred in the local animal facilities and maintained on a 12h dark/light cycle (7am/7pm) with food and water ad libitum. Mice were decapitated and brains were rapidly removed into ice-cold gassed medium (95% O2/5% CO2) containing (in mM): 125 NaCl, 2.5 KCl, 1 MgCl2, 0.4 CaCl2, 1.25 NaH2PO4, 26 NaHCO3 and 25 glucose. Coronal slices of the median part of the hypothalamus (250m), were cut with a HM650V vibratome (Microm, Walldorf, Germany) and placed in a holding chamber at 34°C for 30 min. Slices were then transferred into another incubating chamber at room temperature (22-25°C) continuously perfused at a rate of 1-2ml.min-1 with Phosphate Bicarbonate Buffer Saline (PBBS), pH 7.4 when bubbled with 95% O2/5% CO2, containing additional CaCl2 (final concentration: 2mM) and used for recordings. Solutions were applied to the slices through the perfusion system.

2.1.2 Acquisition System

The acquisition system records bright field image sequences on an upright Axioskop microscope (CarlZeiss, Le Pecq, France) using an ApoChromat 63X/1 water immersion objective. Short sequences of 200 images were captured every minute at a frame rate of 200 frames/second with a GigE Vision color CMOS camera (PicSight, Leutron Vision, Switzerland). To use the camera at its maximum speed, the image size was reduced to acquire a 200x200 pixels sub area of the image. The acquisition and automatic recording of all the successive 1sec sequences was done using StreamPix software (Norpix, Montreal, Canada). This acquisition system was chosen to be used in routine analysis in place of the confocal linescan [13] strategy as it is more sensitive to the focus drifts and the movements of the sample. An image recorded with this system is displayed in Fig. 2 and can be compared with the output of a slow Axiocam Carl Zeiss camera, Le Pecq, France, providing more accurate acquisition in Fig. 1.

2.2 Removal of artifacts

Grid or Fixed Pattern Noise (FPN) in the CMOS sensor is one artifact that should be removed prior to any image processing because it adds artificial information not related to cilia and it biases the realignment of the images. An image frame from the acquisition system is displayed in fig. 2 where the grid is visible. This fixed pattern can be removed assuming that the coefficient [15] and geometrical properties of the grid remain constant. In addition to the CBF estimation algorithm provided in the following, we propose an original FPN removal method well adapted to our acquisition procedure where the coefficient of the FPN is directly

computed from the useful image and using the geometrical features of the FPN. To this aim we consider the acquisition of a background sequence of 200 images (same illumination, without brain slice) and its computed average (AVG). Thus, AVG is supposed to contain only the grid pattern.

It is assumed now that the grid AVG is added to each frame, and consequently to the average (AV) of the 200 images containing the brain slices, up to an unknown constant multiplicative factor α. This factor remains to be estimated in order to subtract the grid efficiently. Regardless the frame, a single line of 200 pixels is considered for this estimation. Let's call $av(n)$ and $avg(n)$ the corresponding lines of AV and AVG, whose respective means have been subtracted and where n stands for the column index. Lines that are free of cilia samples will produce better estimation. Considering the illustrative examples of fig. 2, a line parallel to the border of the sample will be selected for the following computation.

The statistical properties of the line $av(n)$ do not allow an efficient use of a least square method for the estimation. Indeed, with respect to the grid aspect of this FPN, it can be proven that the autocorrelation function of $avg(n)$ exhibits a large spike for lag $m = 0$, i.e. column shift equal 0. Thus, for a guessed value α of the multiplicative coefficient that has to be estimated, the correlation function is computed such as:

$$r(m, \alpha) = \sum_{n=0}^{N-m-1} [av(n) - \alpha.avg(n)]\, avg(n+m) \tag{1}$$

where N stands for the number of pixels of the two lines.

In order to estimate the correct value of the coefficient we propose to use an exhaustive search of the minimum value of the criterion:

$$c(\alpha) = \frac{|r(0,\alpha) - r(1,\alpha)| + |r(0,\alpha) - r(-1,\alpha)|}{|r(1,\alpha)| + |r(-1,\alpha)|} \tag{2}$$

with respect to the parameter α. This criterion tends to be high as long as the grid remains in the line of interest, and low when the grid is perfectly removed.

Once the coefficient has been estimated, the weighted average image AVG containing the grid can be subtracted from each individual frame that contains the beating cilia.

Because of the flux generated by the cilia and the perfusion system, the recorded samples are slowly spatially shifted as long as the experiment lasts. Thus, the corrected images will be realigned before the CBF computation. This image registration stage is crucial in order to get accurate CBF estimation, since a change in the location of the region of interest increases measurement variability. Maximization of the 2-dimensional correlation function of a reference image and each individual frame, based on mean square minimization [16], will be robust with respect to interferences and asymptotically optimal when the noise is Gaussian. In that case, the reference image can be selected as an average of a small set of images, assuming static position. The image alignment is indeed influenced by the static part of the sample and not by the cilia. This implies that the registration will not track the cilia motion because it plays a very small role in frame-by-frame based global image variation.

2.3 Frequency estimation

Here we will briefly describe two methods commonly used to extract the Cilia Beating Frequency based on Fast Fourier Transform (FFT). We then explain in more detail the Maximum Likelihood Estimator (MLE) method we have developed to exploit the video-microscopy image sequences better.

2.3.1 CBF estimation based on direct FFT

A region of interest close to the beating cilia was selected on the image sequences from video-microscopy for the purpose of designing a sub-image for calculations. The most straightforward procedure is to average the pixel intensities in the whole sub-image in order to reduce the acquisition noise [7] [8]. Note that this average could also be accomplished optically [17]. The Fast Fourier Transform (FFT) of the average value was then obtained. An alternative approach consists in averaging the squared modulus of the FFT of the individual pixels in the sub-image. Thus a plot of magnitude vs. frequency is obtained. The frequency with the maximum magnitude is the CBF. This second method was much more computationally costly but more effective. Note that in contrast to the average of pixels, the modulus of the FFT is invariant with respect to delay in the time domain. It is expected that due to its own motion, one cilia affects pixels in a bounded area with a small delay which is a function of the velocity and the inter-pixel distance. This fact is in favor of any spectral approach based on modulus averaging. Despite the optimality of using the squared modulus in the average, as shown in the following, the single modulus is still in use [19].

2.3.2 Maximum Likelihood Estimator of the CBF

Although the behavioral model of single cilia can be well defined [6], the estimation of the CBF based on this model is a difficult task due to the observation itself. This difficulty is explained not only by the presence of artifacts such as acquisition noise and spatial shift of the active ciliated cells but also because of the overlapping multiple cilia. This phenomenon makes the frame by frame tracking of spatial features tedious and consequently hinders the accurate estimation of the CBF. In contrast to this spatial approach, robustness and accuracy are improved by considering temporal and spatial coherence. In other words, we consider that within a region of interest, all pixels share a common temporal feature which is the frame by frame intensity variation, that may be shifted in time. Possibly, pixels could also capture adjacent cilia beating at the same frequency because of the sequential action producing the metachronal, or travelling, wave. Assuming that the variation is periodic and that each pixel records an abrupt intensity variation, we propose a harmonic model that combines the fundamental frequency (f) and the first and second harmonics. Considering that the model should be invariant with respect to time delays, each pixel intensity variation $p_i(t)$ from the total I within the sub-image, is modeled by:

$$p_i(t) = \sum_{j=1}^{3} [\theta_{i,2j-1} cos(2\pi f j t) + \theta_{i,2j} sin(2\pi f j t)] + n_i(t) \tag{3}$$

Where $n_i(t)$ is a white Gaussian error composed by the modeling error and observation noise. In this model, j and θ stand for the harmonic number and weight of the decomposition, respectively. It is worth noticing that pairs of values $(\theta_{i,2j-1}, \theta_{i,2j})$ convey information of both the amplitude of the harmonic and its temporal shift

although the analysis is focused on the frequency (f). For instance, metachronal wave or cilia synchronization could be assessed by using the phase estimated from these pairs. Once the parameters have been estimated, the use of this model is also beneficial for the image denoising and the enhancement of the principal periodic motion of the cilia ensemble. Although not demonstrated here, this image reconstruction could also be used for flagellar waveform analysis since noise and interferences can be removed as well as non-coherent cilia beating. Among all the available estimators, the Maximum Likelihood Estimator (MLE) [18] is selected for its properties with respect to the error. It is assumed here that the error is Gaussian, stationary and uncorrelated spatially and temporally. Considering the I pixels from the sub-image, maximizing the likelihood function is equivalent to minimize the following criteria:

$$J_1 = \sum_{i=1}^{I} \|\mathbf{p}_i - M_f \mathbf{a}_i\|^2 \tag{4}$$

Where $\mathbf{p}_i$ and $\mathbf{a}_i$ stand for the vector formed by the temporal values of pixel i extracted from the successive frames and the parameters vector, respectively. Note that temporal delays introduced by the sequential recording of the motile cilia by adjacent pixels are inherent to the model. Indeed, thanks to trigonometric identities a delay in time will only modify the parameters $(\theta_{i,2j-1}, \theta_{i,2j})$ but not question the relevance of the model. In this model, the parameter f is the fundamental frequency and only the first and second harmonics are taken into account. Then, M_f matrix contains cosines and sines functions defined over the time t_k

(with $t_1 \leqslant t_k \leqslant t_K$) corresponding to the acquisition of the frames such that:

$$M_f = [M_{1.f} \;\; M_{2.f} \;\; M_{3.f}] \tag{5}$$

with

$$M_{j.f} = \begin{pmatrix} cos(2\pi f j t_1) & sin(2\pi f j t_1) \\ \vdots & \vdots \\ cos(2\pi f j t_K) & sin(2\pi f j t_K) \end{pmatrix}$$

Indeed, the criteria J_1 has to be minimized with respect to the set of parameters f and $\mathbf{a}_i$'s. Developing (4), the solution is thus given by the minimization:

$$\begin{aligned} &\left(\hat{\mathbf{a}}_1, \ldots, \hat{\mathbf{a}}_I, \hat{f}\right) \\ &= \arg \min_{\mathbf{a}_1, \ldots, \mathbf{a}_I, f} \sum_{i=1}^{I} \left[\mathbf{p}_i^T \mathbf{p}_i - 2\mathbf{p}_i^T M_f \mathbf{a}_i + \mathbf{a}_i^T M_f^T M_f \mathbf{a}_i\right] \end{aligned} \tag{6}$$

The derivation of the criteria with respect to the vectors $\mathbf{a}_i$ provides the estimated $\hat{\mathbf{a}}_i$'s:

$$\begin{aligned} \hat{\mathbf{a}}_i &= [\hat{\theta}_{i,1}, \hat{\theta}_{i,2}, \hat{\theta}_{i,3}, \hat{\theta}_{i,4}, \hat{\theta}_{i,5}, \hat{\theta}_{i,6}]^T \\ &= (M_f^T M_f)^{-1} M_f^T \mathbf{p}_i \end{aligned} \tag{7}$$

It can be proven that after substituting these solutions in (6), the minimization is finally a maximization with respect to f:

$$\hat{f} = \arg \max_f \sum_{i=1}^{I} \mathbf{p}_i^T M_f (M_f^T M_f)^{-1} M_f^T \mathbf{p}_i \tag{8}$$

Whatever the value of f, the matrix $(M_f^T M_f)^{-1}$ can be approximated by kI, where I stand for the identity matrix and k a constant. Note that for specific values of f this approximation is indeed the equality. Thus (7) is simplified by:

$$\hat{\mathbf{a}}_i = kM_f^T \mathbf{p}_i \tag{9}$$

and (8) can be replaced by:

$$\hat{f} = \arg\max_f \sum_{i=1}^{I} \hat{\mathbf{a}}_i^T \hat{\mathbf{a}}_i \tag{10}$$

In fact, a sum $(\hat{\theta}^2_{i,2j-1} + \hat{\theta}^2_{i,2j})$ with $j = 1, 2, 3$ is equivalent to the squared modulus of the Fourier Transform (FT) at the frequency $j.f$, namely $|FT(\mathbf{p}_i)|^2(j.f)$. Thus the maximization in (8) is equivalent to:

$$\hat{f} = \arg\max_f \sum_{j=1}^{3} \sum_{i=1}^{I} |FT(\mathbf{p}_i)|^2(j.f) \tag{11}$$

The sum of the squared modulus of the fundamental frequency and its harmonics is also called the Compressed Spectrum $CS(f)$. Then, (11) is replaced by:

$$\hat{f} = \arg\max_f \sum_{i=1}^{I} CS_i(f) \tag{12}$$

This last expression allows an easy interpretation of this maximization, using the mentioned approximation. Finally, It is similar to the problem addressed by the average of squared modulus of FFT but with harmonic modeling accounted in the estimation. Furthermore, we show the optimality of such an average as compared to the usual approaches using values introduced empirically and without the squaring operation. In summary, this last solution uses the priors related to the

observation of the motile cilia and can be efficiently computed with FFT through the introduction of the CS . Note that the optimization (12) should be performed over the single parameter f. Sophisticated optimization algorithms are available but with the risk of converging toward a local maxima. We will prefer in the following an exhaustive search over a given range of the f values, allowing the addition of a priori knowledge and fixing the frequency resolution.

2.3.3 Evaluation of methods

In order to compare the frequency (fMLE) estimated with the Maximum Likelihood Estimation (MLE) to the frequency computed with the FFT of averaged pixels (fAPIX) and the average of FFT (fAFFT) two types of evaluation will be proposed based on simulated and real data. In both cases, a sub-image will be defined where the CBF will be computed. From previous trials, the size of 3×17 pixels seems to be a good compromise between a reduction of the noise influence and the focus on single cilium behavior. In addition, the second evaluation will provide an analysis of sub-image location and size influences. In both cases, the range of the exhaustive search for the optimal frequency will be [6-20]Hz with a resolution of 0.01Hz, using a zero padding technique for the FFT, and for the three methods.

2.3.4 Validation on simulated data

In this simulation, an artificial 3×17 pixels image is synthesized in order to mimic single vertical cilium behavior [6] [13]. Each pixel intensity variation is composed by Gaussian shaped peak trains varying from 0 to 1 with a total duration of 1 second and sampled at 200Hz, corresponding to a rate of 200 frames per second.

The time period of the train of peaks is 0.1 second (CBF=10Hz) and the width of the cilium at half of the height is about 6 pixels. The selected cilia sweep velocity is about 500 pixels per second. All these parameters correspond to what is observed in a very clear real acquisition condition. The estimation of the CBF is performed by using the three methods introduced in section 2.3.3 with different levels of Gaussian noise, very similar to the observed one. For each noise level 500 trials are generated in order to compute the Root Mean Square Error (RMSE) to simultaneously assess the bias and the variance of the estimation.

2.3.5 Validation on real data

The ground truth for CBF measurement is not easily provided because the CBF can change with metabolic variations and it is hindered by the cilia overlapping. Moving the location of the sub-image within the global image should be a good strategy to compare the methods, assuming that the CBF should vary only weakly with respect to time and location and that the perfusion medium properties are constant. It is considered that CBF estimation will be performed disregarding the sub-image position and without any memory of preceding positions. Each pixel p_i in the sub-image will define a vector when considering its intensity frame by frame. A sequence of 200 frames corresponding to 1 second (the time is sampled with a frequency equal to 200Hz) is analyzed by using the three approaches: fMLE, fAPIX and fAFFT. As described in section 2.1.1, images captured the ciliated ependymal cells from the third ventricle in mouse brains. In order to analyze the CBF variations, sequences of 200 frames are processed every 10 seconds. So, for a total amount of 6000 frames, 30 estimates of CBF are provided by the above mentioned methods. For this evaluation of CBF, the conditions of the experiment

are constant. Indeed, the full image is not processed as a whole but regions of interest, called sub-image, are used instead. Thus, for each position of the sub-image, defined by the line and column indexes, 30 CBF are computed as illustrated in fig. 5. Since experimental conditions are stable in this part, an almost constant CBF throughout time is expected. This is assessed by using the mean value μ and standard deviation σ of these values. Assuming the estimator is unbiased, the most accurate method should then be characterized by the smallest standard deviation. Note that CBF could change as a function of the sub-image location. Then, the criterion used for performance evaluation will be the standard deviation. In order to confirm the advantage of using a sub-image of several pixels instead of a single one, this test will be performed on 3x17 and 1x1 pixels sizes. The first sub-image size allows not only to track a single cilium but also to include several pixels exhibiting similar intensity profile. This will enable us to use the different CBF estimators. It is worth noting that in almost all cited papers the region of interest is also defined by visual inspection.

2.4 Application

The third ventricle is a brain cavity lined by ciliated ependymal cells and surrounded by the hypothalamus, a brain region particularly involved in the control of metabolism. Besides maintaining a protective barrier, suggested ependymal cell functions include regulation of CSF flow and composition, and local mixing of the CSF to optimize the dispersion of its components [20]. Ependymal cells are speculated to be part of the central glucose sensing system [2] and can store high levels of intracellular glycogen which can be mobilized upon glucose withdrawal [21],

suggesting that the rapid mobilization of energy plays a key role in ependymal cell function in the brain. We investigated whether metabolic changes in the CSF (such as oxygenation, pH and glucose variations) could influence the third ventricle ependymal cell CBF. The forces applied by cilia depend linearly on their frequency [22] and thus the CSF flux is related to the CBF. In this way, CBF changes in response to metabolic variation could contribute to local homeostatic processes by modulating the CSF flux and thus bringing the necessary nutriments to the surrounding cells when needed.

The method proposed in section 2.3.2 is applied to the described slices through 5 different experiments, with sub-image size of 3x17 pixels. A- PBBS obtained with standard preparation was left without 95% O2/5% CO2 bubbling, with pH adjusted to 7.4 with HCl. The solution was changed to the standard PBBS 95% O2/5% CO2-bubbled solution (pH=7.4). B- Effect of a change in solution from the standard 95% O2/5% CO2-bubbled PBBS solution to the un-bubbled PBBS one with the pH adjusted to 7.4. C- The standard 95% O2/5% CO2-bubbled PBBS solution (pH 7.4) was replaced by a 95% O2/5% CO2-bubbled PBBS one with pH adjusted to 8.5 (with NaOH). D- The standard 95% O2/5% CO2-bubbled 25mM glucose PBBS solution (pH 7.4) was replaced by a PBBS 95% O2/5% CO2-bubbled solution (pH 7.4) in which glucose was lowered to 0.1 mM. E- At 34°C, different increasing concentrations of the hypothalamic peptide MCH (melanin concentrating hormone) in PBBS were successively applied for 5 min.

3 Results

For the simulated data, different levels of noise were selected to compare the CBF estimators. Fig. 3 displays the RMSE of the three estimators plotted versus the signal to noise ratio (SNR). It is clear that the MLE outperforms the two other estimators regardless the SNR values. This result shows that the mathematical model based on the MLE optimally takes into account the spatial and spectral properties of the system (cilia movement observed through several pixels, and combination of fundamental frequency and harmonics, respectively). This allows for a lower variance in favour of the MLE, confirmed in the real data by shifting the location of the sub-image. In fig. 4 the initial (line index equal to 84) and final sub-images (line index equal to 55) are displayed (white rectangles) after shifting the position pixel by pixel in column and line directions. This range of values corresponds to positions from close to far from the cell's outer surface. The average trend of the CBF, which is function of the column position, is given in fig. 6 and is calculated as follows. First, for a given position of the sub-image the mean CBF μ is computed from each image sequence number (an example is given fig. 5). Second, these mean values are averaged over the lines 55 to 84 for each available column position. Although the global CBF variations along the columns are similar, the presented methods provide slightly different estimations. This proves that for accurate measurement the methods are not comparable. Besides, it shows that whatever the method the CBF is not constant along the cell's outer surface.

The different performances could also be explain by looking thoroughly within the image sequences. Figure 5, corresponds to the estimated CBF along the sequence number, or time, where the frequency is supposed to be constant during

the recording of the 6000 frames. However, intrinsic physiological variability is plausible but the variation range of fAFFT and fAPIX in fig. 5 seems to be unlikely. fMLE appears more stable than fAFFT and fAPIX, which is expected with respect to the constant medium composition.

This last remark is confirmed by statistically comparing the standard variations σ and the mean μ (computed over the sequence number) of the estimators as a function of the horizontal positions (column from 21 to 179). This comparison is then performed for each vertical position (line from 84 to 55). Table 1 gives the average values of the CBF estimation statistics μ and σ for different vertical positions, computed along the horizontal positions. After a successful normality test, the paired t-test has been applied to compare the σ values of fMLE to fAPIX and fAFFT, namely σ_{fMLE}, σ_{fAPIX} and σ_{fAFFT}. If σ_{fMLE} is significantly lower ($p < 0.01$ after Bonferroni correction) than σ_{fAPIX} and σ_{fAFFT} then a star is added to the table.

It can be noticed that the $\overline{\mu}$ values are quite similar (between 11 and 12Hz) regardless the lines and methods. Besides, the differences between the methods could be explained by the standard deviation $\overline{\sigma}$ of the estimations. It is clear that the standard deviation increases as long as the sub-image moves away from the base of the cilium, but remains statistically lower for $\overline{\sigma_{fMLE}}$. This could be explained by pronounced overlapping effects of different cilia far from the base. This is in good agreement with the result found in the simulations where the fMLE outperforms other estimators. The effect of adding pixels to the model is visible (detailed results not provided here) when comparing all values. What is remarkable is that the fMLE estimator still performs better with only one pixel but with a higher standard deviation than with the 3x17 pixels sub-image ($p < 0.01$ after

Bonferroni correction). This result could be predicted because of the asymptotical efficiency of the MLE, i.e the higher the number of observations, the better the estimation, assuming that the proposed model is still valid when pixels are added. Finally, this result is also in favor of positioning the sub-image in the vicinity of the cilium base and of maintaining it in this position by correcting the image shifts as mentioned in section 2.2.

When applied to real data, the MLE method was successfully used to determine the CBF of ependymal cells boarding the mouse third ventricle in brain slices [11]. In this study, we have shown that the CBF varies from slice to slice between 2 and 16 Hz with an average of 11.18 $\pm$ 0.72 Hz (N=55 slices in 14 mice) and that it is positively modulated by the neurotransmitter serotonin, by ATP and by the hypothalamic peptide Melanin-Concentrating Hormone (MCH). To investigate the influence of metabolic factors such as oxygen, pH and glucose concentration on the CBF of the same ependymal cells, the MLE method was applied to the described slices through the 4 different experiments. As shown in Fig. 7A, an increase in the oxygenation of the perfusion medium induced a decrease in CBF. The CBF percentage variation (measured at the peak of the effect relative to the average baseline before the solution change) was (mean $\pm$ s.e.m) -17.4 $\pm$ 2.50% (t-test, p <0.02, n=5 slices in N= 3 mice). Conversely, oxygen depletion induced an increase in CBF (Fig.7B) of 23.2 $\pm$ 4.88% (t test p <0.02, n=5 slices in N= 3 mice). Similarly, a basification of the extracellular medium (from pH 7.4 to 8.5) induced an increase in CBF of 23.00 $\pm$ 2.54% (t test p <0.02, n=5 slices in N= 3 mice) as illustrated in Fig 7C. Finally, a decrease in the glucose concentration in the medium (from 25mM to 0.1mM) induced a reversible increase of CBF of 19.37 $\pm$ 7.14% (t test p <0.05, n=8 slices in N= 5 mice) as shown in Fig. 7D.

The example presented in Fig. 7E illustrates that it is possible to record higher CBFs. It shows the effects on CBFs recorded at 34°C (thus with a faster baseline CBF) of increasing concentrations of an orexigenic hypothalamic peptide known to be released during fasting, Melanin Concentrating hormone (MCH), which has previously been shown to modulate the CBFs in the third ventricle [11].

4 Discussion

Motivated by the great interest for CBF measurement in the field of Biology, we proposed a novel estimator which optimally takes into account the time and spatial properties of the system. Robustness has been addressed by introducing a harmonic model of the temporal variation of pixel intensities. The presence of harmonics in the spectrum had already been pointed out [10] but was never used before in order to directly improve the CBF estimation. Furthermore, positioning the sub-image over the region of interest, similar to the Line Of Interest (LOI) [13] [9], is still an open question. In the literature, this positioning remains manual as the subsequent processing, and finally subjective. In this paper we have shown that the CBF value is subject to this positioning and we have provided evidence that the choice of the position should be made next to the cell surface in order to reduce the overlapping effect. In the CBF measurement, any estimator exhibiting less variance is preferred. The proposed MLE achieved this task, as shown in the validation section by using simulated and real data. Although outside of the scope of this paper, it has been shown that increasing the size of the sub-image provides a more accurate CBF estimation. However, this property is valid as long as the observed cilia beat synchronously in the sub-image, which is not guaranteed if its size becomes too

large. It is worth noting that amplitudes and frequencies have been assumed to be constant throughout the sequences of 200 frames. A more general extended model could be introduced to overcome this limitation but at the exppense of a lower robustness and a higher computational cost. All referenced papers using visual inspection as the gold standard for the CBF quantification might be limited due to bias and habituation, particularly in long lasting experiments with evolutive conditions.

Next to the removal of image artifacts, the method outputs exhibit lower variability. This positive behavior has been advantageously exploited for the tracking of small and large variations of the CBF in response to chemical changes in the cell bath. This paper puts forward a methodological approach based on real data providing promising results about brain ciliary behavior. Although the method has been applied to images recorded with a microscope it could also be applied to new imaging modalities [23]. As a result of this application, we show in Fig. 7 that ependymal cell CBF accelerates in response to a decrease in oxygen, a basification of the pH, or a decrease in glucose concentration in CSF. Moreover, we confirm that CBF can be modulated by MCH, a hypotalamic orexigenic peptide known to play important roles in the control of metabolism and whose release is increased during fasting [11], including at physiological temperature, when the basal CBF is elevated. Thus Fig. 7 emphasizes that this method can be adequately applied to obtain insights about how CBF are affected by changes in physiology and/or the CSF environment and highlights the success of this technique to probe even small changes in CBF. Altogether, these original results suggest that cilia beating could play a major role in regulating the cerebrospinal fluid flow in response to metabolic changes, and hence in regulating brain metabolism. Their action could

indeed trigger homeostatic protective compensatory feed-back mechanisms providing nutrients to the brain when the levels of those nutrients in the cerebrospinal fluid start decreasing.

Acknowledgement

Authors would like to thank N. Ramkumar, G. Conductier and J.L. Nahon for their contributions to this work and C. Lebeaupin, P. Lowis and P. Bonizzi for their help with the manuscript proofreading. This work has been partly funded by grant PEPS 2010 and supported by INSB.

References

1. Salathe M. Regulation of mammalian ciliary beating. Annu Rev Physiol, 2007; 69:401-422.
2. Garcia MA, et al. Hypothalamic ependymal-glial cells express the glucose transporter GLUT2, a protein involved in glucose sensing. J Neurochem, 2003; 86:709-724.
3. Kim W, Han TH, Kim HJ, Park MY, Kim KS, Park RW. An Automated Measurement of Ciliary Beating Frequency using a Combined Optical Flow and Peak Detection. Health Inform Res., 2011; 17(2):111-9.
4. Yi WJ, Park KS, Lee CH, Rhee CS, Nam SW. Directional disorder of ciliary metachronal waves using two-dimensional correlation map. IEEE Trans Biomed Eng. 2002;49(3):269-73.
5. Yi WJ, Park KS, Lee CH, Rhee CS. Correlation between ciliary beat frequency and metachronal wave disorder using image analysis method. Med Biol Eng Comput., 2003;41(4):481-5.
6. O'Callaghan C, et al. Analysis of ependymal ciliary beat pattern and beat frequency using high speed imaging: comparison with the photomultiplier and photodiode methods. Cilia, 2012; 1(1):8
7. Dimova S, Maes F, Brewster ME, Jorissen M, Noppe M, Augustijns P. High-speed digital imaging method for ciliary beat frequency measurement, Journal of Pharmacy and Pharmacology, 2005; (57): 521-526.

8. Yi WJ, Park KS, Min YG, Sung MW. Distribution mapping of ciliary beat frequencies of respiratory epithelium cells using image processing, Med Biol Eng Comput., 1997; 35(6):595-9.
9. Olm MA, Kogler JE, Macchione M, Shoemark A, Saldiva PH, Rodrigues JC. Primary ciliary dyskinesia: evaluation using cilia beat frequency assessment via spectral analysis of digital microscopy images. J Appl Physiol, 2011; (111):295-302.
10. Oldenburg AL, Chhetri RK, Hill DB, Button B. Monitoring airway mucus flow and ciliary activity with optical coherence tomography. Biomed Opt Express, 2012; 3(9):1978-92.
11. Conductier G, Brau F, Viola A, Langlet F, Ramkumar N, Dehouck B, Lemaire T, Chapot R, Lucas L, Rovère C, Maitre P, Hosseiny S, Petit-Paitel A, Adamantidis A, Lakaye B, Risold PY, Prévot V, Meste O, Nahon JL, Guyon A. Melanin-concentrating hormone regulates beat frequency of ependymal cilia and ventricular volume. Nature Neuroscience, 2013. http://dx.doi.org/10.1038/NN.3401
12. Doyle RT, Moninger T, Debavalya N, Hsu WH. Use of confocal linescan to document ciliary beat frequency. J Microsc., 2006; 223(Pt 2):159-64.
13. Lechtrek KF, Sanderson MJ, Witman GB. High-speed digital imaging of ependymal cilia in the murine brain. Methods in Cell Biol, 2009; (91):255-264.
14. Lechtrek KF, Delmotte P, Robinson ML, Sanderson MJ, Witman GB. Mutations in Hydin impair ciliary motility in mice. The Journal of Cell Biology, 2008; 180(3):633-43.
15. Schoberl M, Fossel S, Kaup A. Fixed pattern noise column drift compensation (CDC) for digital moving picture camera, ICIP, 2010; 573-576.
16. Zitova B, Flusser J. Image registration methods: a survey. Image Vision Comput., 2003; 21(11): 977-1000.
17. Chilvers MA, O'Callaghan C. Analysis of ciliary beat pattern and beat frequency using digital high speed imaging: comparison with the photomultiplier and photodiode methods, Thorax, 2000; (55):314-317.
18. Kay SM. Fundamentals of Statistical Signal Processing. Ed. Prentice Hall, 1993.
19. Smith CM, Djakow J, Free RC, Djakow P, Lonnen R, Williams G, Pohunek P, Hirst RA, Easton AJ, Andrew PW, O'Callaghan C. CiliaFA: a research tool for automated, high-throughput measurement of ciliary beat frequency using freely available software. Cilia, 2012; 1:14.

20. Del Bigio MR. Ependymal cells: biology and pathology. Acta Neuropathol, 2010; 119:55-73.

21. Psarra AM, et al. Immunocytochemical localization of glycogen phosphorylase kinase in rat brain sections and in glial and neuronal primary cultures. J Neurocytol., 1998; 27:779-790.

22. Teff Z, Priel Z, Gheber LA. The forces applied by cilia depend linearly on their frequency due to constant geometry of the effective stroke. Biophys J., 2008; 94:298-305.

23. Liu L., et al. Method for quantitative study of airway functional microanatomy using micro-optical coherence tomography. PLoS One, 2013; 8(1).

Tables

Table 1 averaged μ and σ function of sub-image vertical position. Sub-image size: 3x17 pixels

	Line					
	84	82	80	75	65	55
$\overline{\mu_{fMLE}}$	11.1	11.2	11.2	11.3	11.8	11.4
$\overline{\mu_{fAPIX}}$	11.2	11.2	11.4	11.8	12.0	11.8
$\overline{\mu_{fAFFT}}$	11.3	11.2	11.3	11.6	12.0	11.7
$\overline{\sigma_{fMLE}}$	1.1 *	1.1 *	1.2 *	1.2 *	1.3 *	1.5 *
$\overline{\sigma_{fAPIX}}$	1.5	1.5	1.5	1.5	1.7	1.9
$\overline{\sigma_{fAFFT}}$	1.2	1.3	1.3	1.5	1.6	1.8

Figure Captions

Fig. 1. A single frame containing ciliary beating recorded with an Axiocam camera

Fig. 2. A single frame containing ciliary beating and interferences recorded with a GigE Vision color CMOS camera

Fig. 3. RMSE function of SNR: fAFFT (dotted line), fAPIX (dashed line), fMLE (solid line)

Fig. 4. Image with the first (line 84) and last (line 55) sub-image positions defining regions of interest. The sub-image is shifted along the horizontal axis and for different lines

Fig. 5. CBF within the sub-image centered on line 84 and column 179 : fAFFT (dotted line), fAPIX (dashed line), fMLE (solid line)

Fig. 6. Average trend, or mean of the CBF, computed with the lines 55 to 84 for different column positions: fAFFT (dotted line), fAPIX (dashed line), fMLE (solid line)

Fig. 7. Representative variations of CBF recorded in ependymal cells from mice brain slices at room temperature in response to changes in O2/CO2 (A, B), pH (C) and glucose (D), and to the application of the hypothalamic peptide MCH at 34°C (E). Notice that the baseline CBF before the change in composition of the perfusion medium varied from slice to slice. The variations illustrated here in response to the treatments could be observed in slices with different initial CBF levels and were reversible upon washout. Black bars indicate the duration of application of each respective solution to the slice. Dashed lines indicate the average baseline CBF.

Figures

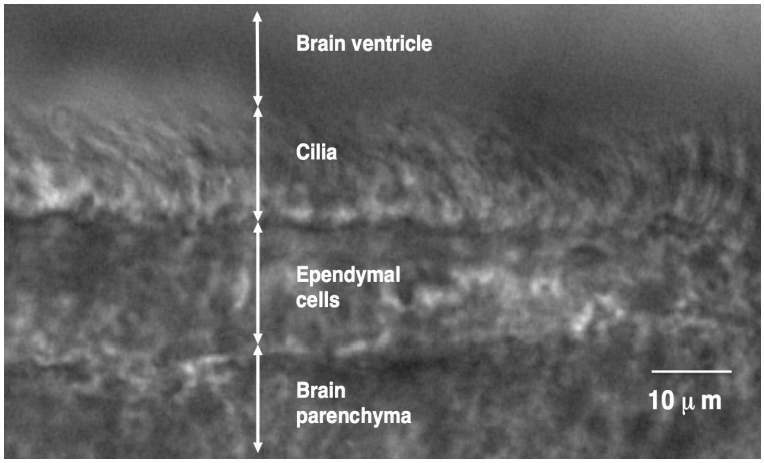

Fig. 1 A single frame containing ciliary beating recorded with an Axiocam camera

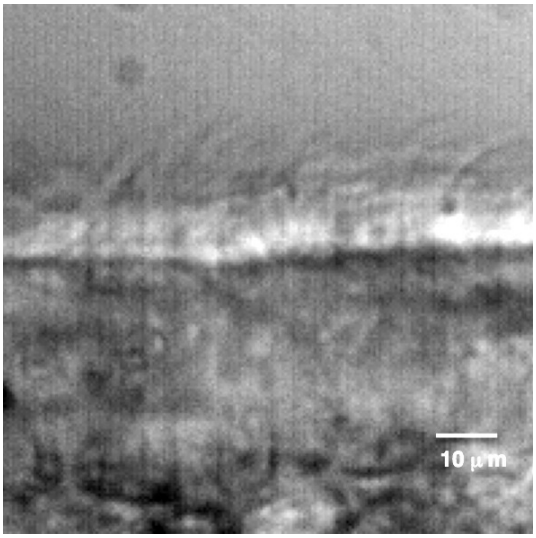

Fig. 2 A single frame containing ciliary beating and interferences recorded with a GigE Vision color CMOS camera

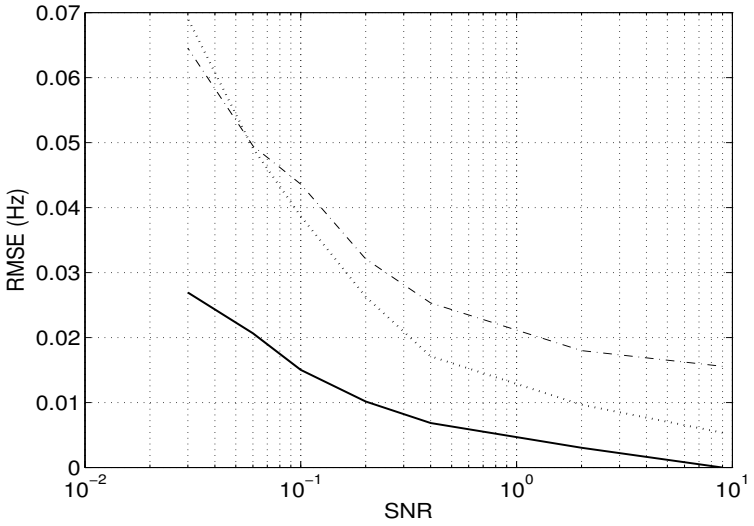

Fig. 3 RMSE function of SNR: fAFFT (dotted line), fAPIX (dashed line), fMLE (solid line)

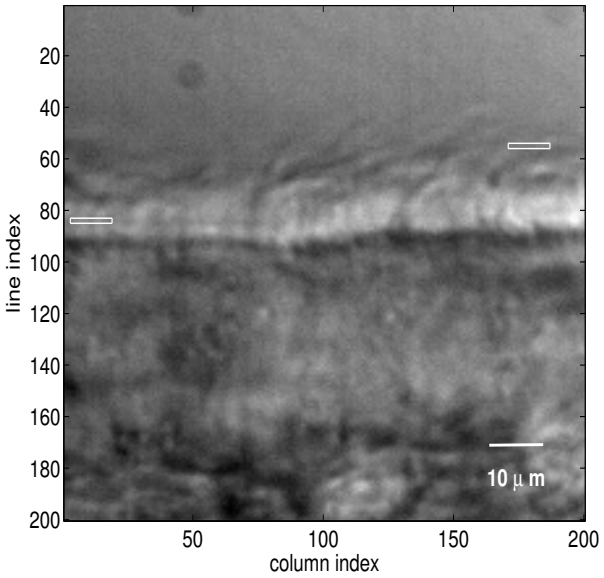

Fig. 4 Image with the first (line 84) and last (line 55) sub-image positions defining regions of interest. The sub-image is shifted along the horizontal axis and for different lines

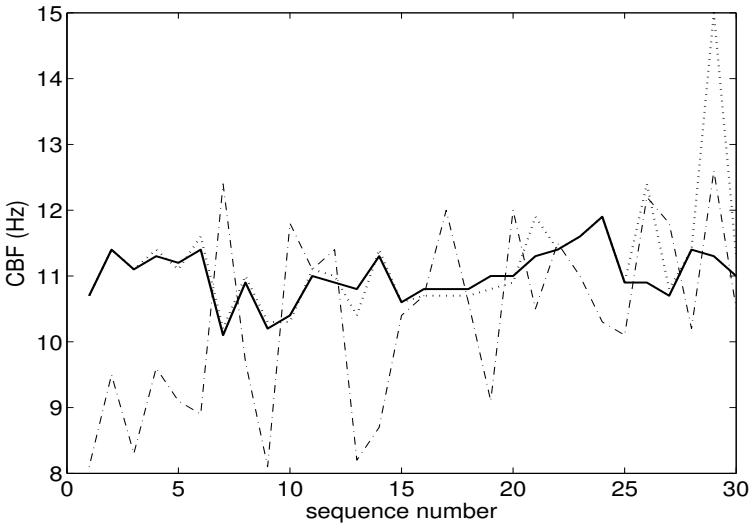

Fig. 5 CBF within the sub-image centered on line 84 and column 179 : fAFFT (dotted line), fAPIX (dashed line), fMLE (solid line)

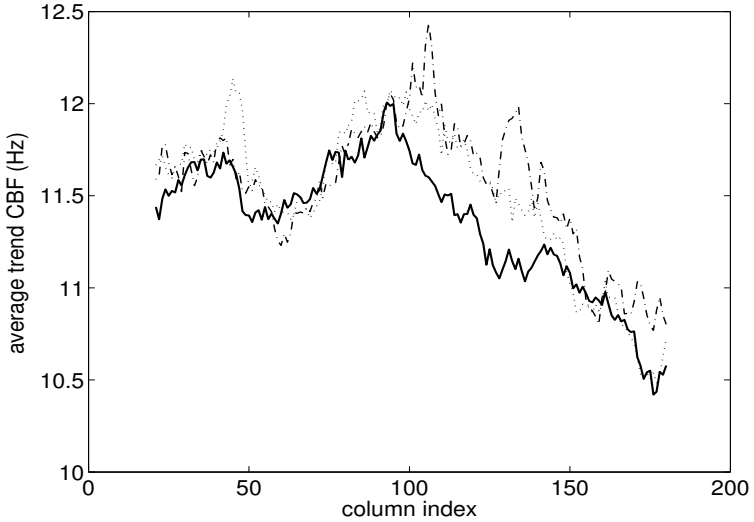

Fig. 6 Average trend, or mean of the CBF, computed with the lines 55 to 84 for different column positions: fAFFT (dotted line), fAPIX (dashed line), fMLE (solid line)

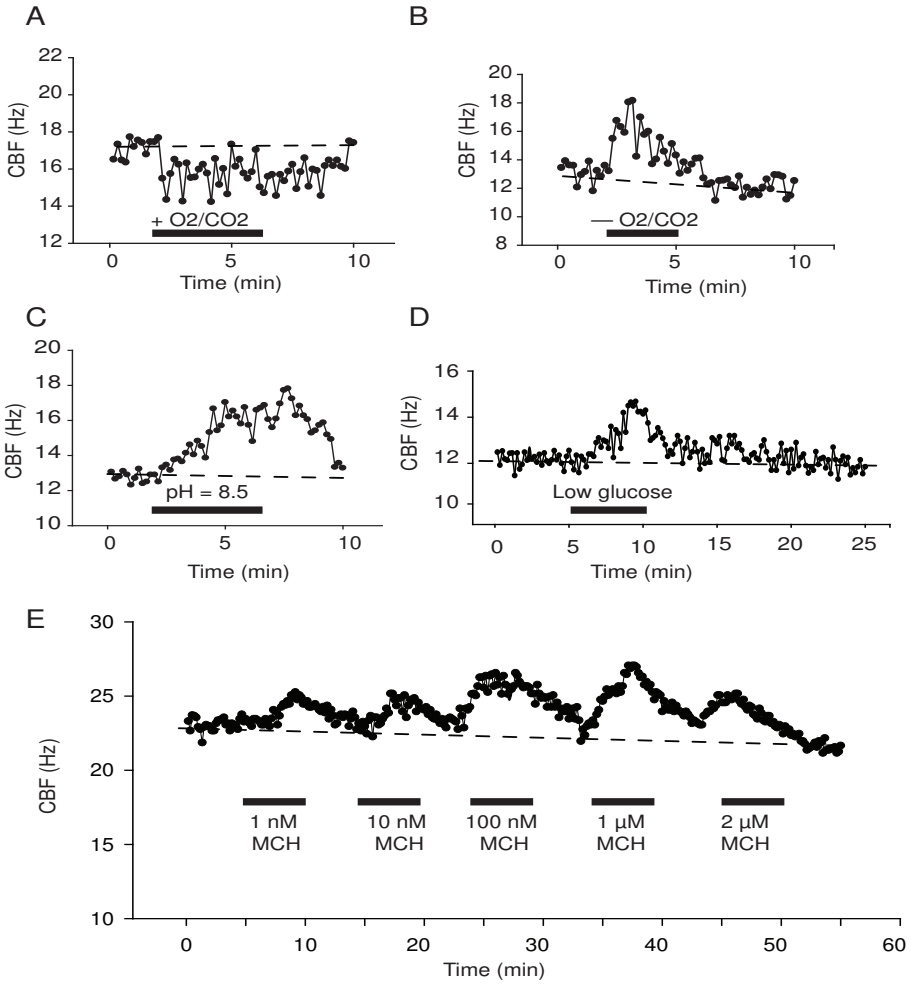

Fig. 7 Representative variations of CBF recorded in ependymal cells from mice brain slices at room temperature in response to changes in O2/CO2 (A, B), pH (C) and glucose (D), and to the application of the hypothalamic peptide MCH at 34°C (E). Notice that the baseline CBF before the change in composition of the perfusion medium varied from slice to slice. The variations illustrated here in response to the treatments could be observed in slices with different initial CBF levels and were reversible upon washout. Black bars indicate the duration of application of each respective solution to the slice. Dashed lines indicate the average baseline CBF.